Journal of Microscopy, Vol. 177, Pt 2, February 1995, pp. 150–161.
Received 8 June 1994; accepted 31 October 1994

Application of confocal laser microscopy and three-dimensional Voronoi diagrams for volume and surface estimates of interphase chromosomes

R. EILS,*¶** E. BERTIN,‡ K. SARACOGLU,¶ B. RINKE,¶ E. SCHRÖCK,†
F. PARAZZA,‡ Y. USSON,‡ M. ROBERT-NICOUD,‡ E. H. K. STELZER,§ J.-M. CHASSERY,‡
T. CREMER†* & C. CREMER¶*

**Interdisciplinary Centre for Scientific Computing (IWR) and **Graduate College 'Modelling and Scientific Computing in Mathematics and Science', University of Heidelberg, INF 368, 69120 Heidelberg, Germany*
†Institute of Human Genetics and Anthropology, University of Heidelberg, INF 328, 69120 Heidelberg, Germany
‡Equipe DyoGen and Lab. TIMC (CNRS URA 1618) Université Joseph Fourier, 38041 Grenoble cedex, France
§European Molecular Biology Laboratory (EMBL), Postfach 102299, D–69012 Heidelberg, Germany
¶Institute of Applied Physics, University of Heidelberg, Albert-Überle-Str. 3–5, 69120 Heidelberg, Germany

Key words. Chromosome territories, three-dimensional tessellation, three-dimensional Voronoi diagram, optical sectioning, volume and surface area estimates.

Summary

This study demonstrates the use of Voronoi tessellation procedures to obtain quantitative morphological data for chromosome territories in the cell nucleus. As a model system, chromosomes 7 and X were visualized in human female amniotic fluid cell nuclei by chromosomal *in situ* suppression hybridization with chromosome-specific composite probes. Light optical serial sections of 18 nuclei were obtained with a confocal scanning laser fluorescence microscope. A three-dimensional (3-D) tessellation of the image volumes defined by the stack of serial sections was then performed. For this purpose a Voronoi diagram, which consists of convex polyhedra structured in a graph environment, was built for each nucleus. The chromosome territories were extracted by applying the Delaunay graph, the dual of the Voronoi diagram, which describes the neighbourhood in the Voronoi diagram. The chromosome territories were then described by three morphological parameters, i.e. volume, surface area and a roundness factor (shape factor). The complete evaluation of a nucleus, including the calculation of the Voronoi diagram, 3-D visualization of extracted territories using computer graphic methods and parameterization was carried out on a Silicon Graphics workstation and was generally completed within 5 min. The geometric information obtained by this procedure revealed that both X- and 7-chromosome territories were similar in volume. Roundness factors indicated a pronounced variability in interphase shape for both pairs of chromosomes. Surface estimates showed a significant difference between the two X-territories but not between chromosome 7-territories.

Correspondence: Christoph Cremer.

Introduction

Recent evidence has demonstrated that chromosomes occupy distinct domains in the cell nucleus, termed chromosome territories (for review see Cremer *et al.*, 1993). Each territory can be considered as a connected, variably-shaped, three-dimensional (3-D) structure which is mutually exclusive from other territories. Individual chromosome territories can be 'painted' by fluorescence *in situ* hybridization with chromosome-specific composite DNA-probes (Lichter *et al.*, 1988; Pinkel *et al.*, 1988). Light optical serial sectioning of nuclei with painted chromosome territories has become possible with the development of confocal scanning laser fluorescence

microscopy (Cremer & Cremer, 1978; Brakenhoff *et al.*, 1985; Stelzer *et al.*, 1986). To estimate first-order stereological quantities like volume, surface area, length and number of optically sectioned objects, appropriate segmentation, clustering and stereological procedures are required.

In spite of recent evidence for differences in the genetic activity of paternally and maternally derived autosome homologues at certain loci, it seems reasonable to assume that such homologues by and large have a similar overall genetic activity. In contrast, in female cells only one of the two X-chromosomes is genetically active (Xa), while its homologue (Xi) is genetically inactive with the exception of a few sites. It has been widely assumed that a much more compacted structure of Xi is associated with (perhaps is responsible for) this difference in genetic activity (Lewin, 1994). Contrary to this assumption, recent estimates of the volumes of the two painted X-territories in nuclei of female human amniotic fluid cells have indicated little, if any, difference (Bischoff *et al.*, 1993; Rinke *et al.*, 1995). In these studies, for segmentation a thresholding procedure was applied to each individual optical section. Subsequently, volumes of the segmented chromosome territories were obtained by the Cavalieri estimator (Gundersen & Jensen, 1987; Webb, 1988).

Stereological methods have been used to obtain unbiased estimates of the surface area of optically sectioned anisotropic objects. The spatial grid (Sandau, 1987) was designed to be applied to sections such as those provided by scanning laser optical sectioning (Howard & Sandau, 1992). The orientator is another designed-based approach (Mattfeldt *et al.*, 1990) which provides estimates of stereological parameters using isotropic sections. All these approaches require a segmentation of the sections and a subsequent clustering, i.e. a description of the topological relationships between structures delineated in different sections. Thresholding procedures have been generally used for segmentation of microscopic objects (Bischoff *et al.*, 1993) and have been combined with 3-D component labelling for clustering (Park & Rosenfeld, 1971; Baumann *et al.*, 1992).

In this study, we have applied an alternative approach for simultaneous truly 3-D segmentation, clustering and determination of first-order stereological parameters based on the construction of Voronoi diagrams. The Voronoi diagram is one of the fundamental data structures in computational geometry and is widely used in a large variety of applications (for a survey see Aurenhammer, 1991; Okabe *et al.*, 1992). Here an approach, initially developed by Bertin *et al.* (1992, 1993), was adapted to perform segmentation, clustering and calculation of morphological parameters of 'painted' territories of chromosome X and 7 in 3-D data sets obtained by serial optical sectioning of human female amniotic fluid cell nuclei. Chromosome 7 was chosen for comparison because of its similar DNA content (2·7%) as compared to the DNA content of the X-chromosome (2·5%) (Morton, 1991). In most nuclei the territories of one chromosome X differed in volume from its homologue by a factor less than 1·5 and likewise for chromosome 7. In contrast, the results indicate a more pronounced difference between the surface areas of the two X-territories as compared to the chromosome 7 territories.

Materials and methods

Cell material

Human amniotic fluid cells with normal female karyotypes (46,XX) were grown on glass slides. These cells typically contain a single nucleus with ellipsoidal shape. After 3 days the cells were fixed for 5 min with buffered formalin (4% formaldehyde solution (Merck) in 1× phosphate-buffered saline, PBS). The slides were treated twice with Triton X-100/Saponin (0·1% each, 5 min), washed in 0·1 M Tris-HCl (pH 7·2), equilibrated in 20% glycerol in PBS for 20 min, freeze-thawed three times by briefly dipping in liquid nitrogen, and stored at 277 K in PBS containing 0·04% sodium azide until use. Prior to *in situ* hybridization, cells were digested with pepsin in 0·01 M HCl, pH 2·0, at 310 K. The extent of digestion was monitored with a standard light microscope and was allowed to proceed until the cytoplasm was largely removed. Post-fixation was carried out for 10 min with 1% formaldehyde solution buffered in PBS.

DNA probes and probe labelling

Chromosome-specific plasmid libraries established from sorted human chromosomes 7 (pBS7) and X (pBSX) were a gift from Dr J. Gray (University of California, San Francisco). Total DNA from these libraries was prepared and nick-translated with Biotin-16-dUTP (Boehringer Mannheim, Germany) (for details see Lichter & Cremer, 1992). The chromosome-7-specific alphoid DNA probe p7t1 (Waye *et al.*, 1987) was a gift from Dr H. F. Willard (Case Western Reserve University, Cleveland, Ohio). Nick-translation of the p7t1 probe was performed with Digoxigenin-11-dUTP (Boehringer, Mannheim, Germany).

Chromosomal in situ suppression (CISS) hybridization

Two-colour fluorescence *in situ* hybridization (FISH) was performed as detailed in Lichter & Cremer (1992) using the biotinylated, composite DNA probes of chromosomes 7 and X and the digoxigenin-labelled chromosome-7-specific alphoid DNA probe. Two microgrammes of DNA from each chromosome library was ethanol precipitated in the presence of 20 μg Cot1 fraction of human DNA (BRL) and 10 μg of salmon sperm DNA (Boehringer Mannheim, Germany). The probe mixture was dried and resuspended in

10 μl hybridization solution (50% formamide, 2 × SSC and 10% dextran sulphate). The DNA was denatured at 348 K for 5 min and allowed to pre-anneal for 30 min at 310 K. Ten nanogrammes of the alphoid DNA probe was added after denaturation as described above without pre-annealing. The pre-treated nuclei were denatured at 345 K for 2 min in 70% formamide and 2 × SSC and dehydrated through an ethanol series (70, 90 and 100%). The probe mixture was then applied to the denatured nuclei under a coverslip (18 mm^2) and sealed with rubber cement. *In situ* hybridization was carried out at 310 K for 16 h. For visualization of the biotinylated probes avidin conjugated to fluoresceine isothiocyanate (FITC, Vector) was used. Dig-11-dUTP-labelled probes were detected by indirect immunofluorescence with mouse anti-digoxin (Sigma) and goat anti-mouse Ig-tetramethylrhodamine isothiocyanate (TRITC) antibodies (Sigma). Nuclei were counterstained with 4'-6-diaminidino-2-phenylindole dihydrochloride (DAPI) for visual inspection of nuclei by conventional fluorescence microscopy. Slides were mounted in PBS/glycerol (1 : 9, v/v) containing 0·1% 1,4-phenylendiaminedihydrochloride as an antifading agent (Serva). Note that any air drying of the cells was carefully avoided throughout the whole procedure to prevent a collapse of the nuclear structure.

Three-dimensional recording of chromosome territories and cell nuclei

Three-dimensional recording (Rinke *et al.*, 1995) was performed using a confocal scanning laser fluorescence microscope built in E. H. K. Stelzer's laboratory (Stelzer *et al.*, 1986; Bischoff *et al.*, 1993). For FITC excitation an argon ion laser at 488 nm was used. TRITC was excited at 543 nm by a helium–neon laser. A Zeiss planapochromat, oil-immersion objective (100×/NA 1·3) with a determined resolution of 250 nm lateral and 500 nm along the optical axis was used (Stelzer, 1990; Stelzer *et al.*, 1991). Prior to optical sectioning the territories of chromosome 7 were visually identified by the TRITC detected signals of the chromosome-7-specific alphoid probe. To obtain a better signal-to-noise ratio each line was scanned 16 times and averaged. For each optical section one FITC fluorescence image of 512 × 512 pixels with 8-bit resolution was recorded. The distance between two subsequent light optical sections was approximately 400 nm. Thus, for each nucleus an image stack of 10 to 20 optical sections was obtained. These data volumes were transferred to a Silicon Graphics Workstation (SGI IRIS INDIGO, R4000, 100 MHz, 80 Mb RAM, Elan Graphics) for image processing and graphic display.

Image analysis

For image analysis an algorithm adopted from computational geometry was used. The basic idea of this algorithm is to tessellate the image into convex polyhedra ('Voronoi polyhedra'), thus building the so-called Voronoi diagram (Preparata & Shamos, 1988; Aurenhammer, 1992; Okabe *et al.*, 1992). Each polyhedron is associated with one creation point ('seed') in the image space and each arbitrary point is assigned to one polyhedron in the Voronoi diagram as follows.

Being $S = \{p_1, \ldots, p_n\}$ the set of seeds in the image space, an arbitrary point in the image space belongs to a certain polyhedron if it is closer to the seed of the respective polyhedron than to any other seed in S. Thus, a polyhedron $\mathrm{Vor}(p_i)$ is defined by all points being closer to its seed p_i than to any other seed $p_j \in S$:

$$\mathrm{Vor}(p_i) = \{x \in R^3 | d(x, p_i) \leqslant d(x, p_j) \forall j \neq i\}$$

where d is the Euclidean distance.

Consequently, the faces ('facets') of a certain Voronoi polyhedron $\mathrm{Vor}(p_i)$ are obtained by the section of all half planes $H(p_i,p_j)$ perpendicular to $\overline{p_i p_j}$ with p_j being a neighbouring seed of p_i:

$$\mathrm{Vor}(i) = \bigcap_{j \neq i} H(p_i, p_j)$$

Thus, $\mathrm{Vor}(p_i)$ is a convex polyhedron with at most $n-1$ facets (Preparata & Shamos, 1988)

The neighbourhood in the Voronoi diagram is described by a second structure, the so-called Delaunay graph, which is dual to the Voronoi diagram. Two seeds, $p_i \in S$ and $p_j \in S$, are neighbours in the Delaunay graph if and only if their associated Voronoi polyhedra $\mathrm{Vor}(p_i)$ and $\mathrm{Vor}(p_j)$, respectively, have one common facet:

$$\mathrm{Del}(S) = \{(p_i, p_j) \in S^2 | \mathrm{Vor}(p_i) \cap \mathrm{Vor}(p_j) \neq \varnothing\}.$$

Thus, the neighbourhood relationship between Voronoi polyhedra is completely contained in the Delaunay graph.

The construction of the Voronoi diagram and the dual Delaunay graph follows the incremental approach (Bertin *et al.*, 1992, 1993). With this approach the image guides the evolution of the Voronoi diagram by adding seeds in those regions of the image space with a high variance of grey values. Since there is no a priori knowledge of the location of the seeds, the Voronoi diagram must be built dynamically:

Initialization. In a first step approximately 30–70 seeds depending on the size of the image volume are randomly placed in the image space according to a Poisson process. For these initializing seeds the Voronoi diagram and the Delaunay graph are built. For each Voronoi polyhedron certain parameters, such as volume, mean and variance of grey values of the voxels belonging to the respective polyhedron, are calculated. Those parameters are used for further refinement of the tessellation.

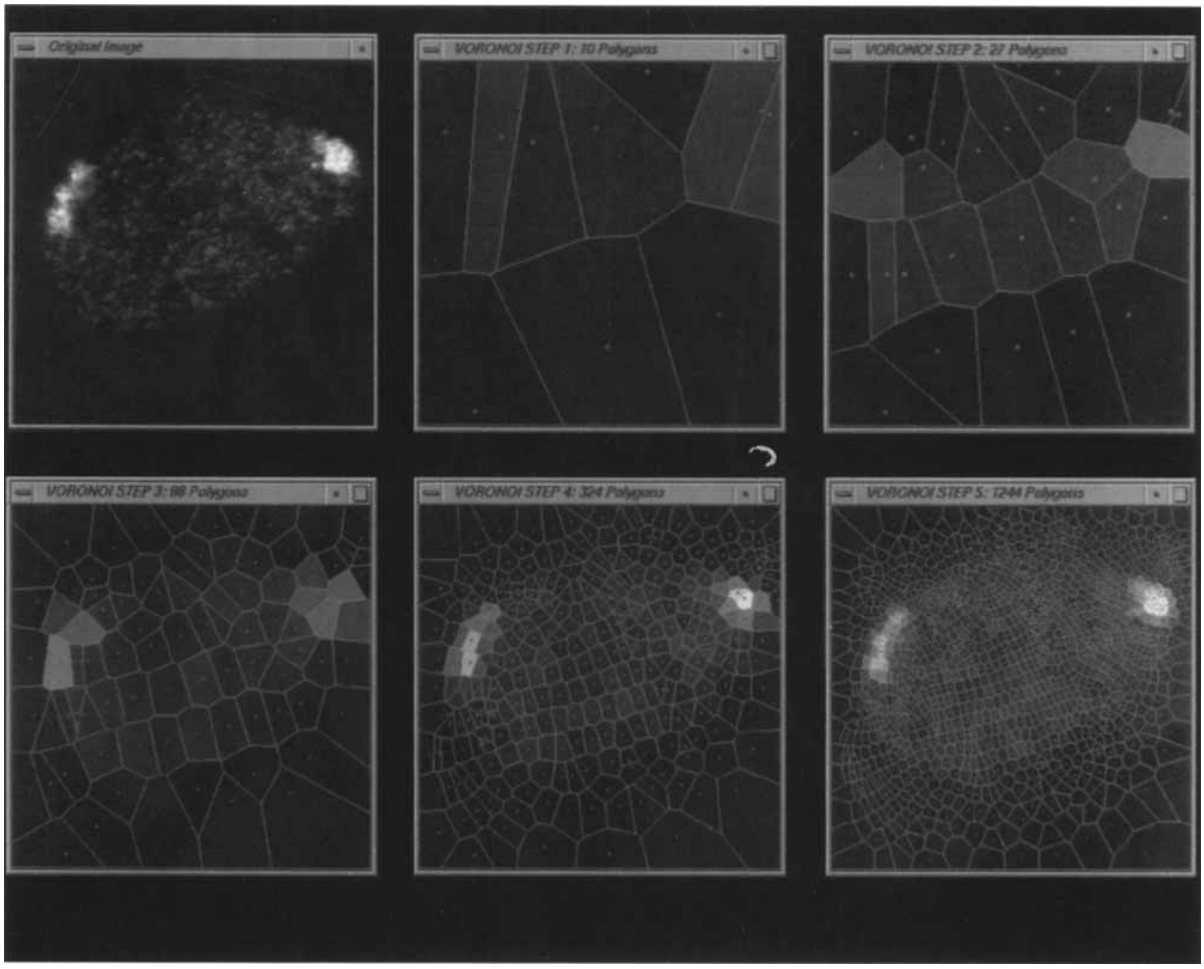

Fig. 1. Application of the iterative Voronoi tessellation procedure to one light optical section of a human amniotic fluid cell nucleus with two painted X-territories. Top left: original image of one section of a nucleus with two painted X-chromosomes. From top middle to bottom right: Voronoi-tessellation steps no. 1 to no. 5. The red dots demonstrate the locations of the seeds of the Voronoi polygons. Note that a 2-D tessellation is demonstrated here for simplicity, while a true 3-D Voronoi tessellation was applied to the stack of light optical serial sections obtained for each nucleus.

Propagation. In the following step, each polyhedron obtained in the previous step is tested for 'homogeneity' (see below). If a polyhedron is homogeneous within the preset limits it must not be further subdivided and is retained. If a polyhedron is still regarded as being inhomogeneous, a new seed is added at the gravity centre of the common facet between two neighbouring inhomogeneous seeds (for a 2-D demonstration see Fig. 1). For the new set of seeds the Voronoi diagram and the Delaunay graph are computed. For each Voronoi polyhedron, the above described parameters are calculated again.

Convergence. The propagation step is iterated until all polyhedra are regarded as being homogeneous. In principle, a wide variety of homogeneity criteria can be chosen. In this study, a polyhedron is regarded as homogeneous if one of the following criteria holds (see Discussion).

1 The standard deviation of the grey value distribution of all voxels belonging to the respective polyhedron is below the overall standard deviation of the grey values of the image volume.

2 The volume of the respective polyhedron is below a preset size (minimum size of a polyhedron = 10 voxels).

After building the Voronoi diagram the tessellated chromosome territories are extracted. For this purpose, a search for polyhedra having connected components under appropriate similarity constraints (see below) is performed in the Delaunay graph. An object is regarded as connected if each polyhedron has at least one facet in common with

another polyhedron belonging to that object. Connected polyhedra which fulfil the same constraints are considered to be similar, i.e. to belong to the same object. Note that this definition of similarity does not imply a similar shape of the polyhedra. Starting with an arbitrary polyhedron in the Voronoi diagram fulfilling the constraint, a search for similar neighbouring polyhedra is performed simultaneously in all directions. Each polyhedron already assigned to an object is labelled to avoid double assignment. For all labelled polyhedra a search for similar neighbouring polyhedra is performed in the same way. This procedure is repeated until no more unlabelled polyhedra can be found belonging to this object. At this stage, the extraction of the first object is finished. Subsequently, another unlabelled, i.e. untreated, polyhedron fulfilling the constraint is searched in the Voronoi diagram. For such a polyhedron, another search connected components is performed in the same way as described above, thus yielding the second object. This procedure is iterated until there are no more unlabelled polyhedra fulfilling the constraint.

There are several possibilities for choosing the similarity criteria, e.g. the mean or gradient of grey values. In this study, two neighbouring polyhedra, i.e. connected vertices in the Delaunay graph, are regarded as being similar, if their respective associated mean grey values exceed a preset threshold. To avoid any subjectivity by interactively choosing a certain grey-value threshold, the chromosome territories are segmented for a wide range of thresholds. For each cell nucleus upper and lower boundaries for the threshold are determined in the following way. The upper limit is set to a threshold value where at least one chromosome territory connected at a lower threshold falls apart into two or more unconnected components (Fig. 2). The lower limit is defined by a threshold where at least one chromosome territory fuses either with another chromosome territory being distinct at a higher threshold or with polyhedra obviously belonging to the background.

Finally, for each threshold chromosome territories were segmented and extracted in the Voronoi diagram without further intervention. For the whole threshold range the total volume of the territory was obtained by adding the volumes of all polyhedra belonging to this object. The volume of a single polyhedron in turn was determined by adding the volumes of all voxels which fell into this polyhedron. The surface area of the territory was obtained by summing the surface areas of all facets which are shared between polyhedra belonging to the object and background polyhedra. The surface area of each individual facet was determined analytically.

To describe the eccentricity of chromosome territories and the roughness of their surfaces we wished to use a dimensionless parameter. Such a parameter, further referred to as the roundness factor (RF), can be defined as

$$RF = 36\pi \frac{V^2}{S^3}; 0 < RF \leqslant 1.$$

It can be regarded as an absolute measure for the relative size of the surface area (S) of an object as compared to its volume (V). Small RF values indicate territories with very extended shape and/or particularly rough surfaces, while an RF value of 1 would describe a sphere with perfectly smooth surface. For each territory volume, surface area and roundness factor estimates were averaged for the whole threshold range. This value was used to calculate the mean values of the respective parameters for the 18 nuclei evaluated in the present experiments. For simplicity these mean values will be further referred to as the volume, surface area and roundness factors, respectively, of a chromosome territory.

For each chromosome territory in each cell nucleus a coefficient of variation was calculated from the single values obtained for the range of thresholds. The variability of a parameter due to threshold variation is described by the mean coefficient of variation (CV), which was obtained by averaging the individual coefficients of all nuclei (cf. Table 1 and Table 2). Similarly, the biological variability in the volume, surface area and roundness factor of a given chromosome territory is described by the coefficient of variation of volume, surface area and roundness factor of the respective chromosome territory in all nuclei. The latter coefficient is further referred to as the overall coefficient of variation (cf. Table 1 and Table 2).

Results

A series of 18 nuclei from female human amniotic fluid cells was studied. In these nuclei the territories of chromosome 7 and X were painted with FITC. The co-localization of the TRITC-labelled chromosome 7 centromeric region with two of the four chromosome territories allowed the discrimination between the territories of chromosomes X and 7. Criteria to choose nuclei were (i) the unequivocal separation of the four chromosome territories and (ii) the intense painting of each territory to facilitate the segmentation of the territory boundaries. For all nuclei, the Voronoi diagram of the 3-D stacks of the images obtained in the FITC channel was built. The resulting Voronoi diagrams comprising the chromosome territories consisted of approximately 3000–7000 polyhedra. The time for computing one Voronoi diagram was about 90 s on the workstation used (Silicon Graphics IRIS INDIGO); the segmentation results were rapidly displayed by Gouraud shading (GL lighting) for performance reasons. The segmentation results for a typical nucleus are demonstrated in Fig. 3 using visualization by ray tracing (Quien & Müller, 1992).

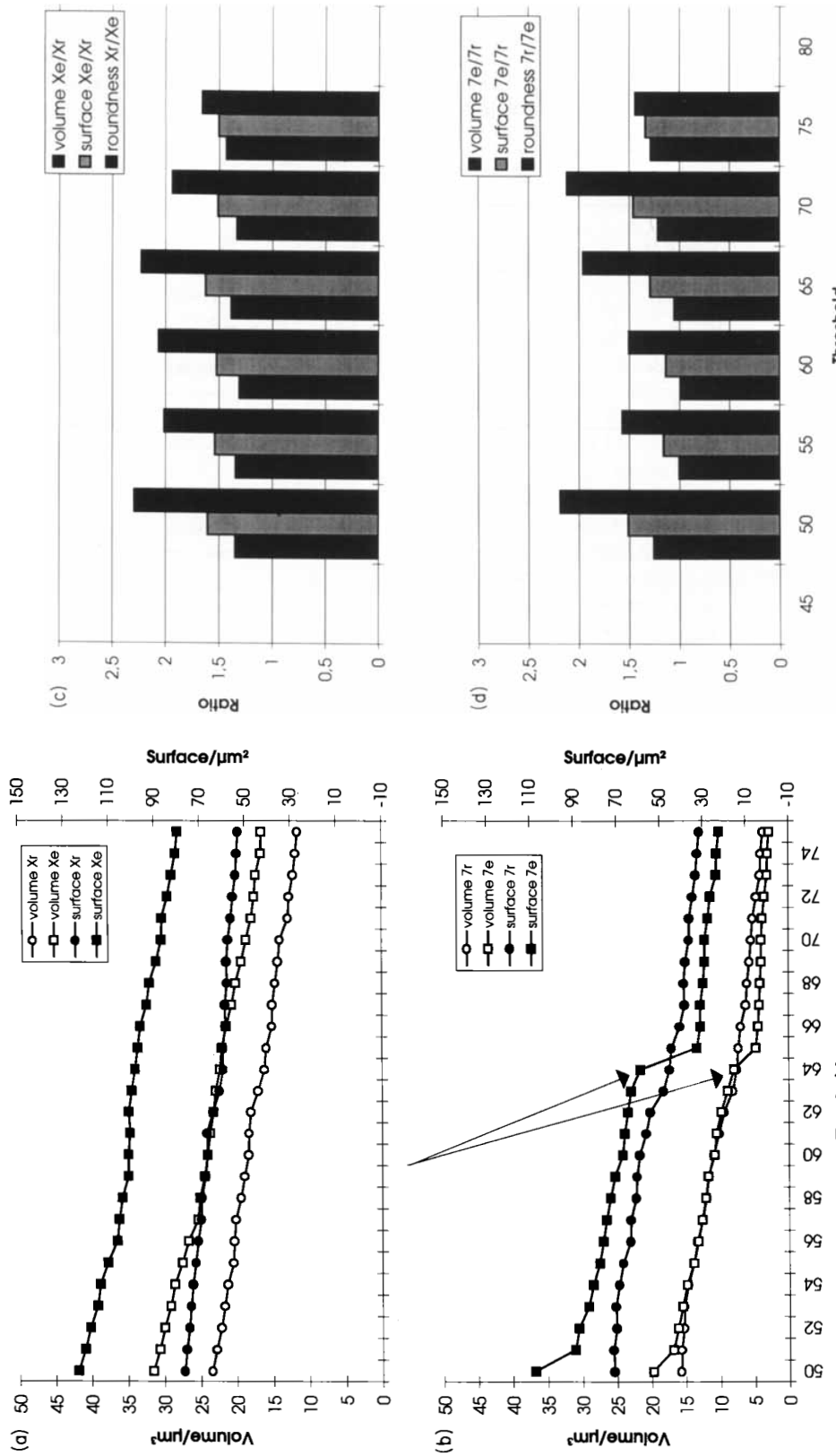

Fig. 2. Graphs of the morphological parameters obtained for chromosome X- and 7 territories in a typical nucleus applying a range of thresholds: (a,b) volume and surface area estimates; (c,d) volume (left column), surface area (middle column) and roundness factor ratios (right column) for each pair of homologues. Note that for thresholds > 65 one of the territories (7e) split into two disconnected regions (for these thresholds only the surface area and volume for the larger of the two regions is shown). For thresholds < 50 one of the territories (7e) fused with background regions. Only the values within the range of thresholds 50–65 were taken for further statistical evaluation; for other nuclei a range of reasonable thresholds was determined accordingly.

Table 1. Mean values of absolute volumes, surface areas and roundness factors for chromosome X-territories (a) and chromosome 7-territories (b); the mean coefficient of variation, the minimum and maximum values obtained in the whole set of nuclei ($n = 18$) and the overall coefficient of variation are presented (for calculations see Materials and methods). The mean coefficient of variation indicates that volume estimates due to threshold variation differ between 30 and 40%, the surface area estimates and roundness factors between 20 and 30%. The overall coefficient of variation indicates that the biological variation of the values obtained in this set of nuclei was some 10%.

(a) Chromosome X

	volume Xe	volume Xr	surface Xe	surface Xr	roundness Xe	roundness Xr
mean	23·3 μm^3	20·7 μm^3	85·7 μm^2	68·7 μm^2	0·097	0·141
mean CV	26·2%	38·2%	21·9%	26·5%	22·7%	16·3%
min.	12·1 μm^3	8·1 μm^3	54·6 μm^2	36·9 μm^2	0·044	0·102
max.	32·7 μm^3	42·2 μm^3	126·0 μm^2	114·8 μm^2	0·138	0·197
overall CV	13·7%	10·6%	7·5%	7·6%	5·2%	4·3%

(b) Chromosome 7

	volume 7e	volume 7r	surface 7e	surface 7r	roundness 7e	roundness 7r
mean	20·2 μm^3	20·9 μm^3	80·7 μm^2	73·3 μm^2	0·082	0·121
mean CV	37·6%	39·2%	26·9%	31·0%	29·3%	33·1%
min.	7·6 μm^3	8·6 μm^3	41·4 μm^2	44·5 μm^2	0·048	0·075
max.	35·5 μm^3	43·2 μm^3	120·2 μm^2	134·3 μm^2	0·153	0·188
overall CV	14·9%	13·4%	7·4%	9·0%	9·8%	6·6%

Following the construction of the Voronoi diagram, upper and lower boundary thresholds for the extraction of the chromosome territories were determined interactively (see the section on image analysis). Subsequently, the chromosome territories were extracted over the whole range of thresholds. At each threshold the volume, surface area and roundness factor (for definition see Materials and methods) were calculated for each extracted territory. For each pair of homologues in a given cell nucleus the territories with the larger roundness factor were termed Xr and 7r, respectively, while the homologous, more eccentric territories were termed Xe and 7e. For each pair Xe/Xr and 7e/7r volume and surface ratios were calculated accordingly. A roundness factor ratio was obtained by dividing the factor for the rounder territory by the factor for the more eccentric territory. According to this assignment the ratio of the roundness factor is always larger than 1. This parameterization step took between 2 and 5 min for a given nucleus depending on the range of thresholds, image size and image information. Note that in accordance with the criteria described in Materials and methods (cf. Fig. 2) only those values which fell into the preset range of thresholds were taken for further statistical evaluation.

Figure 3 shows the 3-D visualization of chromosome territories in a typical nucleus. Table 1 summarizes the absolute values of volume, surface area and roundness factor estimates, while Table 2 presents the respective ratios for homologous territories. Xe had a slightly larger volume than Xa in 11 nuclei and a considerably larger surface area in 14 nuclei. Accordingly, the mean values of the volume and surface area ratios for the two X-chromosome territories were 1·21 and 1·33, respectively. The morphological difference between the two X-chromosome territories is further expressed by the mean of the ratios of the roundness factor being 1·59. For chromosome 7 territories, 7e had a larger volume in nine and a larger surface area in 12 nuclei. The mean volume ratio was 1·02, the mean surface area ratio 1·18 and the mean ratio of roundness factor 1·62.

Figure 4 presents the cumulative curves for volume (Fig. 4a), surface area (Fig. 4b) and roundness factor estimates (Fig. 4c) for both the X- and the 7 territories. Applying the Kolmogorov–Smirnov two-sample test (Young, 1977), no significant difference was obtained between the volumes of Xe and Xr or 7e and 7r (confidence level $P > 0·1$). While the surface estimates for 7e and 7r also did not reveal a significant difference, a highly significant difference was observed for the surface estimates of Xe and Xr (confidence level $P < 0·001$). Highly significant differences were noted for the roundness factors obtained for both pairs of homologues.

Table 2. Mean values of volume ratios, surface area ratios and roundness factor ratios obtained for each pair of chromosome X-territories (a) and chromosome 7-territories (b); the mean coefficient of variation, the minimum and maximum values obtained for such pairs in the whole set of nuclei (n = 18) and the overall coefficient of variation of all nuclei are presented (for calculations see Materials and methods). The mean coefficient of variation indicates that ratio values due to threshold variation differ by some 10%. The overall coefficient of variation indicates that the biological variation of the ratio values obtained in this set of nuclei was some 30%.

(a) Chromosome X

	volume ratio	surface ratio	roundness factor ratio
mean	1·21	1·33	1·59
mean CV	7·8%	7·5%	15·5%
min. ratio	0·52	0·65	1·01
max. ratio	1·63	1·93	3·54
overall CV	32·8%	21·9%	39·8%

(b) Chromosome 7

	volume ratio	surface ratio	roundness factor ratio
mean	1·02	1·18	1·62
mean CV	11·0%	8·7%	19·3%
min. ratio	0·47	0·60	1·01
max. ratio	1·97	1·55	3·87
overall CV	33·3%	14·1%	41·7%

Discussion

The 3-D reconstruction of intranuclear structures such as chromosome territories from light optical serial sections so far has been largely based on the segmentation of each individual section. Subsequently, the series of 2-D-delineated structures have to be recombined into a 3-D structure. The surface area and volume can then be estimated by appropriate algorithms, such as first-order stereological procedures. In the present study, a true 3-D segmentation procedure based on the Voronoi tessellation of 3-D images was used to investigate the morphology of chromosome territories. In this approach segmentation and clustering were performed simultaneously for the whole stack of nuclear sections by building the 3-D Voronoi diagram and its dual, the Delaunay graph. Surface area and volume of intranuclear objects, such as chromosome territories, can then easily be calculated from the surface area and volume of the polyhedra belonging to the respective object.

The time to build the Voronoi diagram and the Delaunay graph for one 3-D data set consisting of 512 × 512 × 20 voxels was approximately 90 s on a Silicon Graphics workstation. The complete analysis of the morphological parameters, which were obtained for the painted territories in a given cell nucleus, was generally completed in 5 min or less. In conjunction with the possibility of rapid visualization and animation of the segmented territories, this method provides a suitable instrument for the morphological analysis of nuclear structures.

In the present report, the Voronoi tessellation procedure was used specifically to study the 3-D morphology of chromosomes 7 and X in human, female amniotic fluid cell nuclei. The chromosome territories were delineated by fluorescence *in situ* hybridization and subsequently recorded by optical serial sectioning with a confocal scanning laser fluorescence microscope. Following the construction of the Voronoi diagram, the chromosome territories were extracted by searching for connected components in the Delaunay graph under threshold constraints and the morphological parameters for each single chromosome territory were calculated. The results indicate that absolute values obtained for a given chromosome territory due to threshold variation differ by some 30–40%, while ratio values differ only by some 10%. These findings indicate the usefulness of the present approach to study relative differences of chromosome territories within the same nucleus. A similar range for chromosome 7 and X-territory volumes was also obtained by the Cavalieri estimator, which may be considered as the gold standard for unbiased volume estimates (Bischoff *et al.*, 1993; Cremer *et al.*, 1993; Rinke *et al.*, 1995; R. Eils & B. Rinke, unpubl. data).

Similar volumes obtained for the two chromosome 7-territories are compatible with the view that a similar overall genetic activity of two homologues should be correlated with a similar state of compaction. In contrast, the finding that similar volumes were also estimated for the two X-territories in female cell nuclei argues against the view that differences in the overall compaction are a major factor to explain the strong differences in the genetic activity (e.g. Lewin, 1994). This view does not exclude that local differences in chromatin compaction play an important functional role but were not ascertained by the present volume measurements.

Several studies have indicated that the active X-chromosome territory (Xa) has a more extended shape than the inactive territory (Xi) (Walker *et al.*, 1991; Bischoff *et al.*, 1993). Based on these findings it appears reasonable to assume that most active X-territories belonged to the class of the more eccentric X-territories (Xe). Differences in surface areas and volumes were significantly less pronounced for pairs of chromosome 7-territories than for the two X-territories (data not shown). At present it cannot be decided whether pronounced differences between the surfaces of the two X-territories results simply from a larger variability in the shape of both X-territories or points

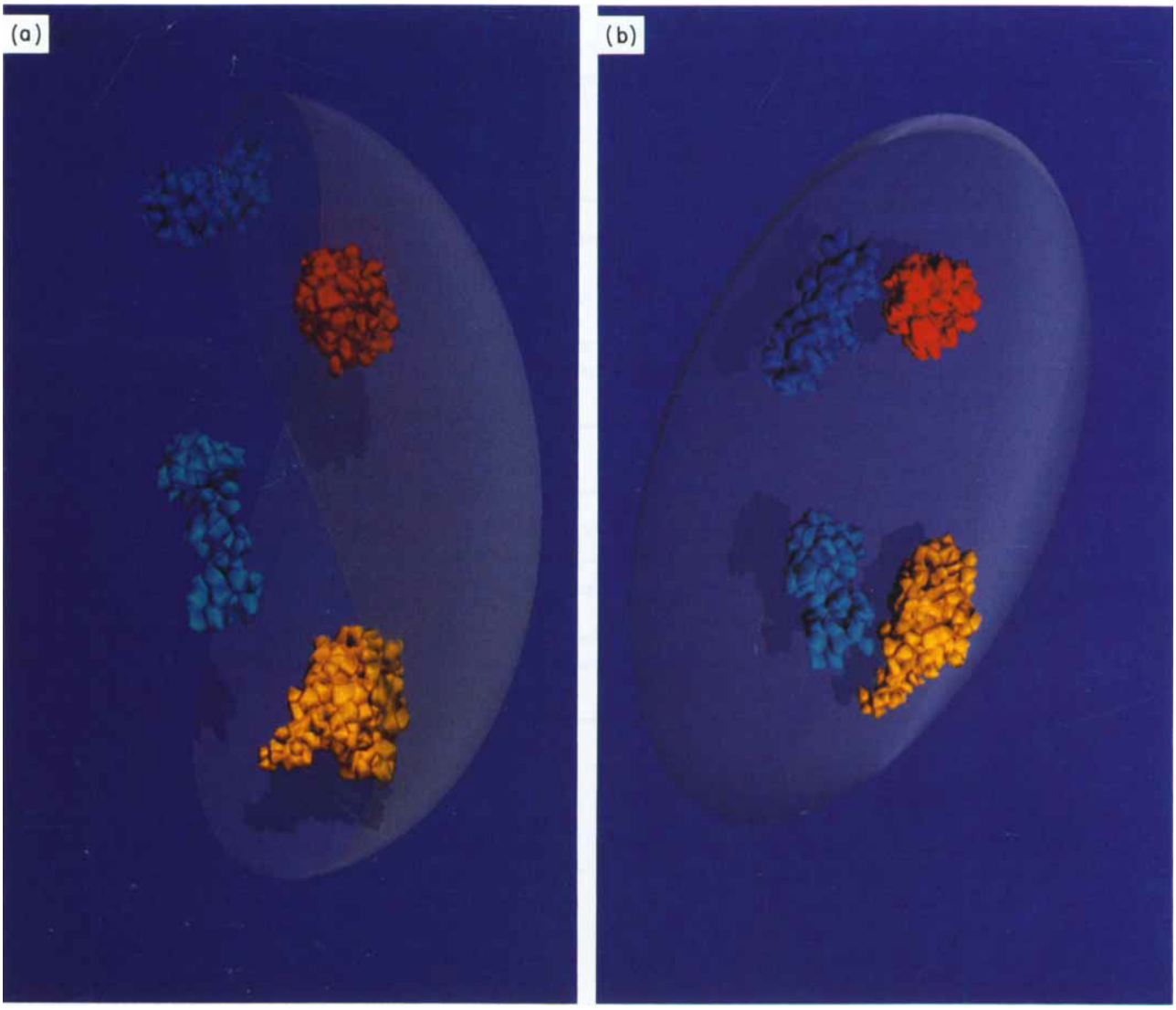

Fig. 3. Computer graphic visualization of the segmented chromosome territories of a typical cell nucleus by ray tracing (for morphological parameters, compare Fig. 2). The extracted territories are false coloured in red (Xr), yellow (Xe), light blue (7r) and dark blue (7e) and viewed in the x-y-direction (a) or x-z-direction (b). The cell nucleus was modelled by an ellipsoid. Since the nucleus was not counterstained in this experiment, the size of the ellipsoid reflects the average size of amniotic fluid cell nuclei measured in other experiments.

to a significantly larger surface area of Xa as compared to Xi. To distinguish between these possibilities it is necessary to discriminate between Xa- and Xi-territories by an additional parameter, such as Barr body staining. Such experiments are presently under way (R. Eils *et al.*, unpubl. data). These studies should help to decide which morphological parameters can best discriminate between active and inactive X-chromosome territories. The direct comparison with autosome territories evaluated in a larger set of nuclei will help to define the extent of morphological differences between the two X-territories as compared to homologous autosome territories in more detail. A discussion of the possible biological implications of surface area differences between chromosome territories needs to be postponed until such data are available. Here we will focus on a discussion of present limitations and possible improvements of both image processing and image acquisition procedures.

The influence of the segmentation procedure itself on the estimates of morphological parameters has to be considered. Care was taken to avoid contributions of background fluorescence to segmentation by an appropriate choice of the lower threshold range. Additionally, in the case of

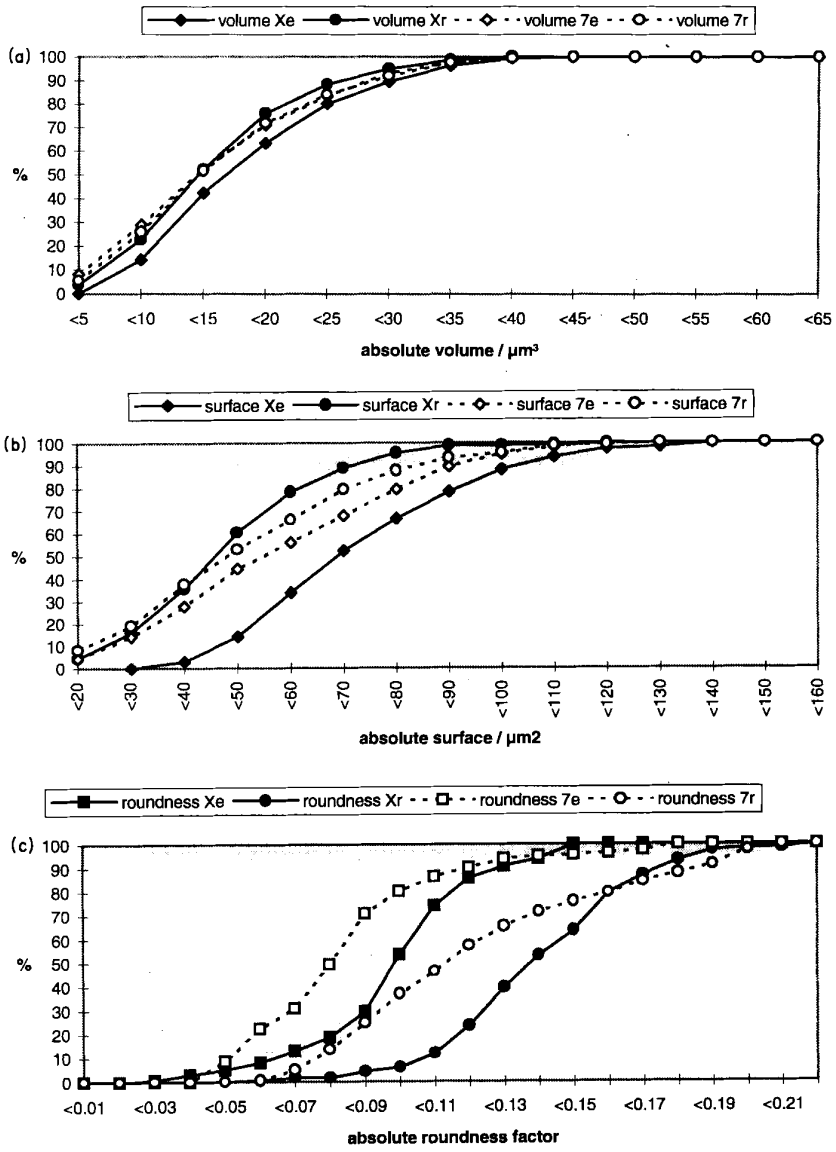

Fig. 4. Cumulative graphs of (a) volumes, (b) surface areas and (c) roundness factors obtained for chromosome X- and 7-territories in the evaluated set of 18 human, female amniotic fluid cell nuclei. Differences between the volumes of Xe and Xr or 7e and 7r were not significant ($P > 0{\cdot}1$) according to the Kolmogorov–Smirnov two-sample test. Differences between the surface areas were highly significant for Xe and Xr ($P < 0{\cdot}001$), but not significant for 7e and 7r ($P > 0{\cdot}1$). The differences between the roundness factors were highly significant for both chromosome X- and chromosome 7-territories ($P < 0{\cdot}001$).

heterogeneities in the painting of a chromosome territory, the Voronoi tessellation procedure may be more stable than a pixel-orientated thresholding procedure due to the spatial properties of the Voronoi polyhedra allowing a considerable variance of image information inside each polyhedron. In this study, we have addressed the problem of reliable volume and surface area estimates. It can be expected that the Voronoi tessellation provides an appropriate method for an estimate of the volume. Aberrations in the determination of the volume might be due to mismatching the true object boundary, which only slightly contributes to the total object volume. In this case, the volume estimation should be nearly unaffected by the geometrical properties of the tessellation procedure.

In contrast, effects of the geometrical properties of the Voronoi tessellation on the surface area estimates might be more pronounced. Segmentation of simulated spherical and ellipsoidal objects as well as microscopical objects of a known size, such as fluorescent spherical beads, resulted in an increase in surface area of generally less than 10%. This overestimation is explained by the fractal nature of the surface obtained by the Voronoi tessellation.

Chromosome territories may obtain a very complex shape, which implies the possibility of complex foldings of its surface from the outside toward the inner space of the territory. The possible extent of underestimation or overestimation of the surface area of chromosome territories due to the limited resolution of both the image acquisition

system and the tessellation procedure is presently unknown and requires further experiments. The resolution was possibly insufficient to determine extensive foldings of chromosome territory surface areas properly. In this case, the calculated surface areas are considered to reflect a lower estimate.

Fuzzy territory boundaries make it difficult to distinguish between foreground and background voxels. We attempted to reduce this ambiguity by applying a region-orientated tessellation procedure. In addition, ratios of morphological parameters were averaged over a wide range of reasonable thresholds. This approach appears to be justified with regard to the small variance of the ratio values over the whole range of thresholds (Table 2).

Care was taken to make the tessellations sufficiently fine in order to avoid a systematic smoothing, i.e. underestimation of the surface area, induced by the geometrical properties of the Voronoi tessellation. The choice of the parameters controlling the evolution of the Voronoi diagram guaranteed that the smallest image unity (one Voronoi polyhedron) was not larger than the resolution provided by the image recording system (250 nm lateral, 500 nm axial) or, alternatively, that the variance of grey values within such a polyhedron was not larger than the total variance (noise) of the whole image (see section on Image analysis).

If objects such as single genes with a size close to the resolution of the image acquisition system are visualized by FISH, the resulting size and extension of such small structures strongly depends on the threshold used for segmentation. The application of deconvolution procedures prior to segmentation may help to 'sharpen' the edges of objects with dimensions close to the resolution limit. There is a strong need for FISH procedures with improved signal-to-noise ratios and for sophisticated criteria different from thresholding for the recognition of connected components in the Voronoi diagram. Studies of both problems are currently being undertaken in our laboratories.

If we consider the possibility of a complex chromosome territory surface structure with important functional implications (Cremer *et al.*, 1992; Zirbel *et al.*, 1993), the low resolution along the optical axis is a major drawback. Because of the thickness of nuclei, near-field scanning optical microscopy (Betzig & Trautman, 1992) cannot be applied to intact nuclei. The axial resolution of confocal fluorescence microscopes may be improved by increasing the aperture of the illuminating light cone (Cremer & Cremer, 1978). Recently, confocal 4Pi-microscopes using two opposing lenses of high aperture for illumination and/or detection have been developed and have yielded a full-width half-maximum (FWHM) value of the point spread function in the z-direction down to 75 nm (Hell & Stelzer, 1992; Hell *et al.*, 1994a,b). In these types of far field microscopes, the strong reduction of the FWHM occurs in the axial direction only. Theoretical considerations (Hell, 1994) indicate that using a two-photon excitation mode confocal arrangement (i.e. dropping the implicit Abbe condition of 1 photon absorption), a lateral FWHM of 75 nm also seems feasible. An improved spatial 3-D resolution of certain object points, e.g. closely adjacent genes visualized by FISH, can also be obtained by devices which allow the tilting of nuclei by given angles (axial tomographic microscopy; Bradl *et al.*, 1992). Rotating devices (0–360°) for digital image acquisition using high-aperture lenses have been implemented for different types of Abbe fluorescence microscopes and confocal scanning laser microscopes (Bradl *et al.*, 1994). These improvements in the resolution of far-field light microscopy in conjunction with Voronoi diagrams and appropriate multicolour fluorescence *in situ* hybridization of entire chromosome territories, subterritories and individual genes should allow much more detailed topological studies of the 3-D conformation of chromosome territories.

Acknowledgments

The excellent support in computer graphics by the Numerical Geometry group at the IWR, University of Heidelberg, and the excellent technical assistance of M.-C. Meffert are gratefully acknowledged. The present work was supported by the Deutsche Forschungsgemeinschaft (DFG, Cr 59/14–3; DFG Cr 60/11–1) and the European Community (GENO-CT 91–0029 (SSMA), CA-AMCA (PL 921307)). R.E. and B.R. are recipients of a fellowship of the Graduate College Program of the Deutsche Forschungsgemeinschaft.

References

Aurenhammer, F. (1991) Voronoi diagrams – a survey of a fundamental geometric data structure. *ACM Computing Surveys*, **23**, 345–405.

Baumann, P.H., Schormann, T. & Jovin, T.M. (1992) Three-dimensional component labelling of digital confocal microscope images: enumeration of replication centres in BrdUrd labelled fibroblasts. *Cytometry*, **13**, 220–229.

Bertin, E., Marcelpoil, R. & Chassery, J.M. (1992) Morphological algorithms based on Voronoi and Delaunay graphs: microscopic and medical applications. *Image Algebra and Morphological Image Processing III*, pp. 356–357. San Diego.

Bertin, E., Parazza, F. & Chassery, J.M. (1993) Segmentation and measurement based on 3D Voronoi diagram: application to confocal microscopy. *Comput. Med. Imag. Graph*, **17**, 175–182.

Betzig, E. & Trautman, J.K. (1992) Near-field optics: Microscopy, spectroscopy, and surface modification beyond the diffraction limit. *Science*, **257**, 189–194.

Bischoff, A., Albers, J., Kharboush, I., Stelzer, E.H.K., Cremer, T. & Cremer, C. (1993) Differences of size and shape of active and inactive X-chromosome domains in human amniotic fluid cell nuclei. *J. Micr. Res. Tech.* **25**, 68–77.

Bradl, J., Hausmann, M., Ehemann, V., Komitowski, D. & Cremer, C. (1992) A tilting device for three-dimensional microscopy: application to *in situ* imaging of interphase cell nuclei. *J. Microsc.* **168**, 47–52.

Bradl, J., Hausmann, M., Schneider, B., Rinke, B. & Cremer, C. (1994) A versatile 2Pi-tilting device for fluorescence microscopes. *J. Microsc.* **176**, 211–221.

Brakenhoff, G.J., van der Voort, H.T.M., van Spronsen, E.A., Linnemans, W.A.M. & Nanninga, N. (1985) Three dimensional chromatin distribution in neuroblastoma nuclei shown by confocal scanning laser microscopy. *Nature*, **317**, 748–749.

Cremer, T., Kurz, A., Zirbel, R., Dietzel, S., Rinke, B., Schröck, E., Speicher, M.R., Mathieu, U., Jauch, A., Emmerich, P., Scherthan, H., Ried, T., Cremer, C. & Lichter, P. (1993) The role of chromosome territories in the functional compartmentalisation of the cell nucleus. *Cold Spring Harb. Symp. Quant. Biol.* **58**, 777–792.

Cremer, C. & Cremer, T. (1978) Considerations on a laser-scanning-microscope with high resolution and depth of field. *Microsc. Acta*, **81**, 31–44.

Gundersen, H.J.G. & Jensen, E.B. (1987) The efficiency of systematic sampling in stereology and its prediction. *J. Microsc.* **147**, 229–263.

Hell, S. & Stelzer, E.H.K. (1992) Fundamental improvement of resolution by a 4Pi confocal fluorescence microscope using two-photon excitation. *Opt. Comm.* **93**, 277–282.

Hell, S., Reiner, G., Cremer, C. & Stelzer, E.H.K. (1993) Aberrations in confocal fluorescence microscopy induced by mismatches in refractive index. *J. Microsc.* **169**, 391–405.

Hell, S. (1994) Improvement of lateral resolution in far field fluorescence light microscopy by using 2-photon excitation with offset beams. *Opt. Comm.* **106**, 19–24.

Hell, S., Stelzer, E.H.K., Lindek, S. & Cremer, C. (1994a) Confocal microscopy with an increased detection aperture: type-B 4Pi confocal microscopy. *Opt. Lett.* **19**, 222–224.

Hell, S., Lindek, S., Cremer, C. & Stelzer, E.H.K. (1994b) Measurement of the 4Pi-confocal point spread function proves 75 nm axial resolution. *Appl. Phys. Lett.* **64**, 1335–1337.

Howard, C.V. & Sandau, K. (1992) Measuring the surface area of a cell by the method of the spatial grid with a CLSM – a demonstration. *J. Microsc.* **165**, 183–188.

Lewin, B. (1994) *Genes V*. Oxford University Press, Oxford.

Lichter, P. & Cremer, T. (1992) Chromosome analysis by non-isotopic *in situ* hybridization. *Human Cytogenetics. A Practical Approach*, 2nd edn, Vol. 1 (ed. by D. E. Rooney and B. H. Czepulkowski), pp. 157–192. IRL Press, Oxford.

Lichter, P., Cremer, T., Borden, J., Manuelidis, L. & Ward, D.C. (1988) Delineation of individual human chromosomes in metaphase and interphase cells by in situ suppression of hybridization using recombinant DNA libraries. *Hum. Genet.* **80**, 224–234.

Mattfeldt, T., Mall, G., Gharehbaghi, H. & Möller, P. (1990) Estimation of surface area and length with the orientator. *J. Microsc.* **159**, 301–317.

Morton, N.E. (1991) Parameters of the human genome. *Proc. Natl. Acad. Sci.* **88**, 7474–7476.

Okabe, B., Boots, B.& Suguhara, K. (1992) *Spatial tessellations – Concepts and Applications of Voronoi Diagrams*. John Wiley, New York.

Park, C.M. & Rosenfeld, A. (1971) Connectivity and genus in three dimensions. *Technical Report TR–156*. University of Maryland.

Pinkel, D., Landegent, J., Collins, C., Fuscoe, J., Segraves, R., Lucas, J. & Gray, J.W. (1988) Fluorescence *in situ* hybridization with human chromosome-specific libraries: Detection of trisomy 21 and translocations of chromosome 4. *Proc. Natl. Acad. Sci.* **85**, 9138–9142.

Preparata, J.P. & Shamos, M.I. (1988) *Computational Geometry. An Introduction*. Springer-Verlag, New York.

Quien, N. & Müller, W. (1992) Gothic vaults and transputers. *IEEE Computer Graphics & Applications*, **12**, 12–13.

Rinke, B., Bischoff, A., Meffert, M.C., Scharschmidt, R., Hausmann, M., Stelzer, E.H.K., Cremer, T. & Cremer, C. (1995) Volume ratios of painted chromosome territories 5, 7 and X in female human cell nuclei studied with confocal laser microscopy and the Cavalieri estimator. *Bioimaging* (in press).

Sandau, K. (1987) How to estimate the area of a surface using a spatial grid. *Acta Stereol.* **6/III**, 31–36.

Stelzer, E.H.K. (1990) The intermediate optical system of laser-scanning confocal microscopes. *Handbook of Biological Confocal Microscopy* (ed. J. B. Pawley), pp. 93–103. Plenum Press, New York.

Stelzer, E.H.K., Marsman, H.J.B. & Wijnaendts van Resandt, R.W. (1986) A setup for a confocal scanning laser interference microscope. *Optik*, **73**, 30–33.

Stelzer, E.H.K., Merdes, A., de Mey, J. (1991) Konfokale Fluoreszenzmikroskopie in der Zellbiologie. *Biologie in unserer Zeit*, **21**, 19–25.

Visser, T.D., Oud, J.L. & Brakenhoff, G.J. (1992) Refractive index and axial distance measurements in 3-D microscopy. *Optik*, **90**, 17–19.

Walker, C.L., Cargile, C.B., Floy, K.M., Delannoy, M. & Migeon, B.R. (1991) The Barr body is a looped X chromosome formed by telomere association. *Proc. Natl. Acad. Sci.* **88**, 6191–6195.

Waye, J.S., England, S.B. & Willard, H.F. (1987) Genomic organization of alpha satellite DNA on human chromosome 7: evidence for two distinct alphoid domains on a single chromosome. *Mol. Cell. Biol.* **7**, 349–356.

Webb, S. (1988) *The Physics of Medical Imaging. Medical Science Series*. Adam Hilger, Bristol.

Young, E.T. (1977) Proof without prejudice: use of the Kolmogorov-Smirnov test for the analysis of histograms from flow systems and other sources. *J. Histochem. Cytochem.* **25**, 935–941.

Zirbel, R.M., Mathieu, U.R., Kurz, A., Cremer, T. & Lichter, P. (1993) Evidence for a nuclear compartment of transcription and splicing located at chromosome domain boundaries. *Chromosome Res.* **1**, 93–106.

Journal of Microscopy, Vol. 177, Pt 2, February 1995, pp. 162–170.
Received 17 May 1994; accepted 2 November 1994

PHOEBE, a prototype scanning laser-feedback microscope for imaging biological cells in aqueous media

T. L. WONG, S. L. SABATO & A. BEARDEN*
Graduate Group in Biophysics and Division of Neurobiology, Department of Molecular & Cell Biology, University of California at Berkeley, Berkeley, CA 94720-3206, U.S.A.

Key words. Scanning confocal interference microscopy of biological cells, laser-feedback interferometry and microscopy, far-field optics.

Summary

Based on the principle of laser-feedback interferometry (LFI), a laser-feedback microscope (LFM) has been constructed capable of providing an axial (z) resolution of a target surface topography of ~ 1 nm and a lateral (x, y) resolution of ~ 200 nm when used with a high-numerical-aperture oil-immersion microscope objective. LFI is a form of interferometry in which a laser's intensity is modulated by light re-entering the illuminating laser. Interfering with the light circulating in the laser resonant cavity, this back-reflected light gives information about an object's position and reflectivity. Using a 1-mW He–Ne ($\lambda = 632{\cdot}8$ nm) laser, this microscope (PHOEBE) is capable of obtaining 256×256-pixel images over fields from ($10\,\mu m \times 10\,\mu m$) to ($120\,\mu m \times 120\,\mu m$) in ~ 30 s. An electromechanical feedback circuit holds the optical pathlength between the laser output mirror and a point on the scanned object constant; this allows two types of images (surface topography and surface reflectivity) to be obtained simultaneously. For biological cells, imaging can be accomplished using back-reflected light originating from small refractive-index changes (>0·02) at cell membrane/water interfaces; alternatively, the optical pathlength through the cell interior can be measured point-by-point by growing or placing a cell suspension on a higher-reflecting substrate (glass or a silicon wafer). Advantages of the laser-feedback microscope in comparison to other confocal optical microscopes include: the simplicity of the single-axis interferometric design; the confocal property of the laser-feedback microscope (a virtual pinhole), which is achieved by the requirement that only light that re-enters the laser meeting the stringent frequency, spatial (TEM_{00}), and coherence requirements of the laser cavity resonator mode modulate the laser intensity; and the improved axial resolution, which is based on interferometric measurement of optical amplitude and phase rather than by use of a pinhole as in other types of confocal microscopes.

*To whom correspondence should be addressed.

1. Introduction

Improving the lateral and axial resolution of light microscopy has been a goal of optical research for many decades. During the past 10 years, the availability of small, but powerful, computers and the development of nanoscale technology has produced significant improvements in resolution for both far-field optical microscopy, through the use of scanning confocal designs, and near-field microscopy, which takes advantage of techniques originating in scanning tunnelling and atomic force microscopy. Interference microscopy, in principle, is capable of measuring optical phase to a small fraction of a wavelength, but it has often been difficult to realise these advantages in practice (Krug, 1964) because of the complexity of optical components, difficulties in alignment, and overall light budget problems. These difficulties can be overcome by use of a simple, single optical-axis form of interferometry in which the laser acts as a coherent light source, interferometric (optical phase and amplitude) detector and amplifier.

The steady-state output intensity of a laser is modulated by the introduction of coherent optical feedback into the laser resonant cavity (King & Steward, 1963; Ashby *et al.*, 1965; Rudd, 1968; Wheeler & Fielding, 1972; Bershtein & Stepanov, 1973). The modulation is dependent on the optical phase and amplitude of the laser light re-entering the cavity. Factors that affect the light re-entering the laser include the reflectivity of the object, which determines the optical amplitude and the total optical pathlength